

Superconductivity at epitaxial LaTiO_3 - KTaO_3 interfaces

D. Maryenko,^{1, a)} I. V. Maznichenko,² S. Ostanin,² M. Kawamura,¹ K. S. Takahashi,¹ M. Nakamura,¹ V. K. Dugaev,³ E. Ya. Sherman,^{4, 5} A. Ernst,^{6, 7} and M. Kawasaki^{1, 8}

¹⁾RIKEN Center for Emergent Matter Science (CEMS), Wako 351-0198, Japan

²⁾Institute of Physics, Martin Luther University Halle-Wittenberg, 06120 Halle, Germany

³⁾Department of Physics and Medical Engineering, Rzeszów University of Technology, 35-959 Rzeszów, Poland

⁴⁾Department of Physical Chemistry and EHU Quantum Center, University of the Basque Country, 48940, Leioa, Spain

⁵⁾Ikerbasque, Basque Foundation for Science, Bilbao, Spain

⁶⁾Institute for Theoretical Physics, Johannes Kepler University, 4040 Linz, Austria

⁷⁾Max Planck Institute of Microstructure Physics, D-06120 Halle, Germany

⁸⁾Department of Applied Physics and Quantum-Phase Electronics Center (QPEC), The University of Tokyo, Tokyo 113-8656, Japan

(Dated: 16 May 2023)

Design of epitaxial interfaces is a pivotal way to engineer artificial structures where new electronic phases can emerge. Here we report a systematic emergence of interfacial superconducting state in epitaxial heterostructures of LaTiO_3 and KTaO_3 . The superconducting transition temperature increases with decreasing the thickness of LaTiO_3 . Such behavior is observed for both (110) and (111) crystal oriented structures. For thick samples, the finite resistance developing below the superconducting transition temperature increases with increasing LaTiO_3 thickness. Consistent with previous reports, the (001) oriented heterointerface features high electron mobility of $250 \text{ cm}^2 \text{V}^{-1} \text{s}^{-1}$ and shows no superconducting transition down to 40 mK. Our results imply a non-trivial impact of LaTiO_3 on the superconducting state and indicate how superconducting KTaO_3 interfaces can be integrated with other oxide materials.

INTRODUCTION

Interfaces between materials can harbor electronic structures distinct from the bulk constituents. One instance is the formation of a metallic layer at the junction of two insulators. A broadly celebrated example is LaAlO_3 / SrTiO_3 interface, that harbors not only high mobility carriers but can also become superconducting at around 300 mK^{1–3}. This rather well controlled system became a fertile testbed to explore two-dimensional superconductivity. In such a strongly asymmetric heterostructure, it was straightforward to assay the role of spin-orbit coupling (SOC) for the superconducting phase, albeit the conduction band is formed by 3d-orbitals of titanium with a moderate SOC energy on the order of 40 meV^{4–7}. In fact, it is anticipated that a sizable spin-orbit coupling can be favorable for unconventional Cooper pairing and for realization of Majorana states^{8–12}. Therefore the recent observation of superconductivity in KTaO_3 , whose conduction band is formed by 5d Ta orbitals with a much larger SOC energy of about 300 meV, may provide a new twist in the formation of superconducting phase in two dimensions. Furthermore, by taking into consideration that bulk KTaO_3 has not still been demonstrated to become superconducting, the emergence of interfacial superconductivity in such a system can provide a distinct insight into Cooper pair formation mechanism¹³. Being isostructural to SrTiO_3 , perovskite oxide KTaO_3 is a quantum paraelectric and has a band gap of about 3.6 eV. The conduction band around Γ point is split by a large spin-orbit coupling in well separated bands with an effective total angular

momentum $J = 1/2$ (higher energy) and $J = 3/2$ states (lower energy).

The first observation of interfacial KTaO_3 superconductivity dates back to experiments with the ionic liquid gating technique, that has revealed a superconducting transition at 50 mK for (001)-oriented KTaO_3 surface¹⁴. Recently the emergence of superconductivity at (110)- and (111)-oriented KTaO_3 surfaces is demonstrated in the majority of cases by growing a EuO layer or depositing amorphous LaAlO_3 layer^{15–21}. The cubic lattice structure of EuO with a lattice constant $a = 5.145 \text{ \AA}$ matches neither (110) nor (111) orientation of KTaO_3 crystal structure, resulting in the formation of either polycrystalline or defective layers at the interface^{16, 17}. Superconductivity was also observed in (111)-oriented KTaO_3 heterostructure with a 10 nm thick $\text{La}_{2/3}\text{Sr}_{1/3}\text{MnO}_3$ top layer²². To have full control over the emergent superconducting state, it is important to have excellent control over the interface's electronic properties, which also includes understanding of the role of the top layer for the emergent phenomena. This control paves the way for integrating superconducting KTaO_3 interfaces with other oxide materials.

Here, we report the emergence of superconductivity in epitaxial grown structures of LaTiO_3 on (110) and (111) oriented KTaO_3 . We observe that the superconducting transition temperature increases with decreasing thickness of the LaTiO_3 layer. For thick samples, the resistance R_{xx} remains finite below superconducting transition temperature and this R_{xx} value increases with increasing LaTiO_3 thickness. These observations indicate a non-trivial impact of LaTiO_3 on the interface's electronic properties. Our finding may facilitate engineering of the superconducting phase at the interface. Bulk LaTiO_3 is a Mott insulator with orthorhombic crystal structure and lattice parameters $a = b = 5.595 \text{ \AA}$ and $c = 7.912 \text{ \AA}$. Therefore,

^{a)}Electronic mail: maryenko@riken.jp

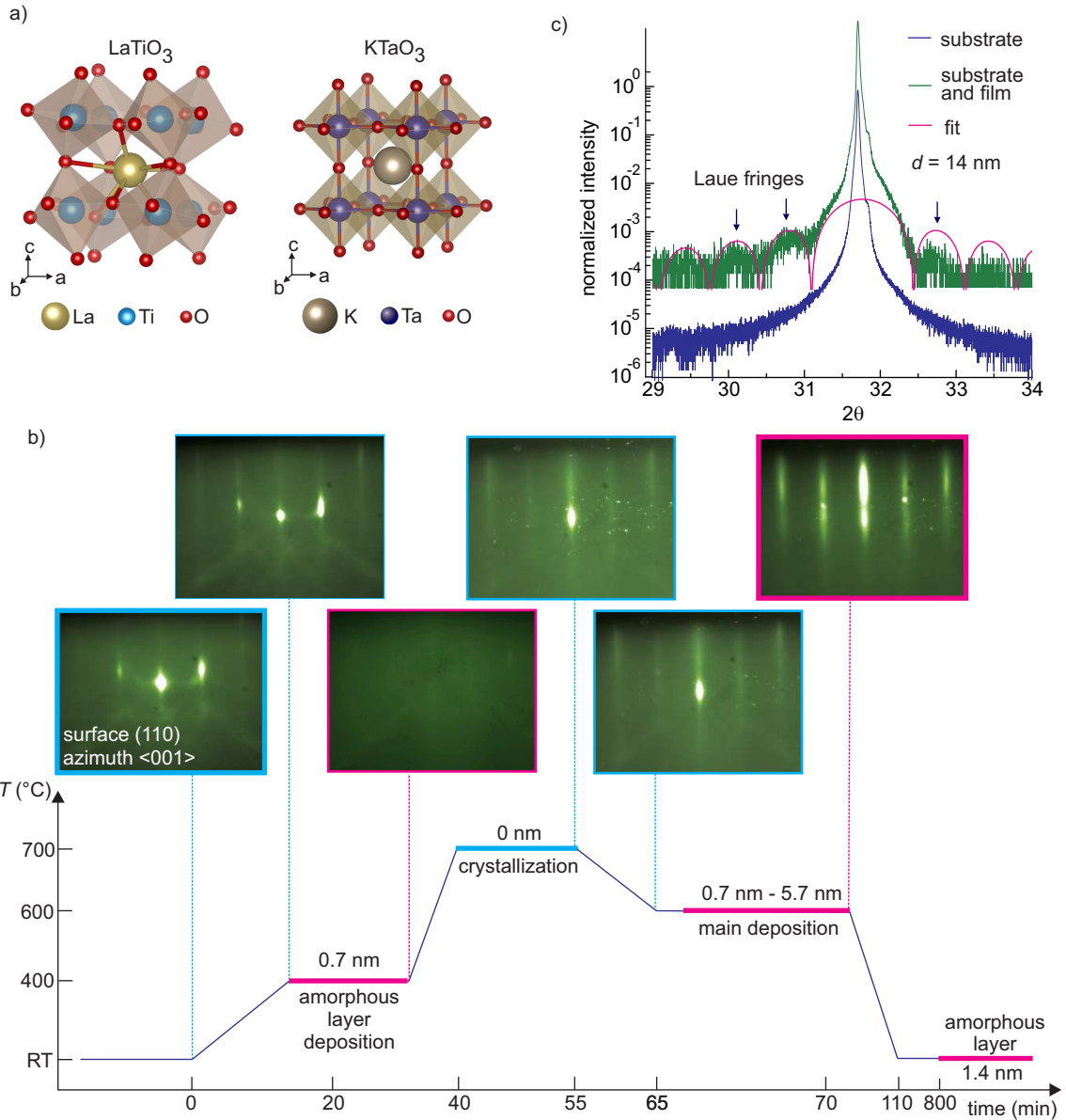


FIG. 1. a) Crystal structure of LaTiO₃ and KTaO₃²³. b) Epitaxial growth process steps for LaTiO₃/KTaO₃ heterostructures. Shown are RHEED patterns at various steps of (110) oriented structure growth. Similar evolution of RHEED pattern with temperature is also observed for structures grown on (001) and (111) KTaO₃ crystal orientations. c) X-ray diffraction patterns (110)-oriented substrate (blue trace) and film on substrate(green trace). The diffraction pattern are shifted for clarity along vertical axis. Red line is the best fit describing the position of Laue fringes.

LaTiO₃ can be thought as a quasi cubic structure with an effective lattice constant $\sqrt{a^2 + b^2}/2 \cong c/2 = 3.956 \text{ \AA}$, which thus differs by only about 0.1% from the lattice constant of cubic KTaO₃ $a = b = c = 3.989 \text{ \AA}$. This facilitates the growth of LaTiO₃/KTaO₃ heterostructure on the three main facets of a cubic crystal system, i.e. (001), (110), and (111)²⁴.

RESULTS AND DISCUSSION

A. Epitaxial growth

LaTiO₃/KTaO₃ structures are grown using pulsed laser deposition technique. A piece of KTaO₃ substrate with a size of about 3 mm x 3 mm was attached to the substrate holder using silver epoxy. A polycrystalline La₂Ti₂O₇ target is ablated in vacuum with a repetition rate of 2 Hz and a laser fluence 1.6 Jcm^{-2} . The growth chamber is equipped with a reflection high-energy electron diffraction (RHEED) monitor allowing

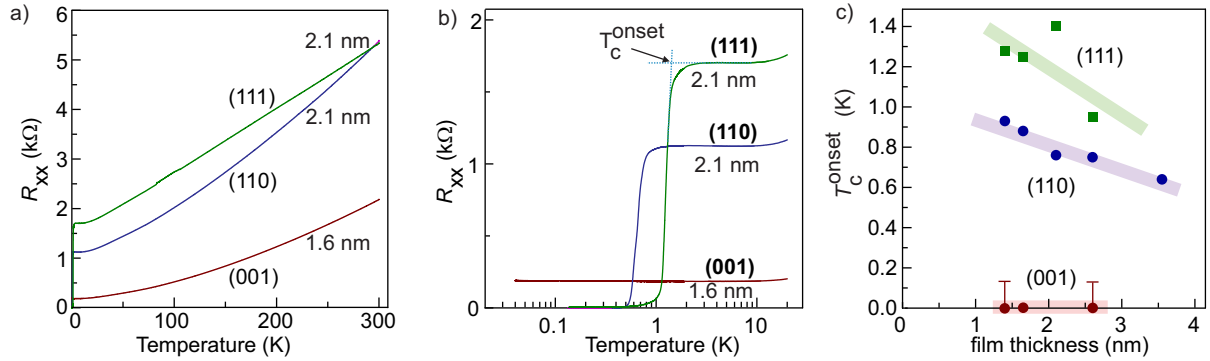


FIG. 2. a) Exemplary temperature dependence of resistance for $\text{LaTiO}_3/\text{KTaO}_3$ heterostructures defined on (001), (110) and (111) crystal surfaces. b) Superconducting state is observed for (110) and (111) oriented heterostructures, while (001) structure remains metallic down to 40 mK. Shown is the definition of the superconducting onset temperature T_c^{onset} . c) T_c^{onset} decreases with increasing the thickness of LaTiO_3 . We assign an error bar of 150 mK for (001)-oriented heterostructures, that are not measured in dilution refrigerator. Thick lines are guides to the eye.

us to observe the growth process *in-situ*. Figure 1b depicts exemplary RHEED patterns during the growth process of (110)-oriented structure. After loading the substrate in the growth chamber, the substrate is heated to 400°C. During this heating step no change in the RHEED pattern is observed. In fact, the atomic force microscopy measurements show that the surface morphology barely changes at 400°C (see Supplementary Information). To prevent the degradation of KTaO_3 surface upon further heating and to suppress the formation of defects, the substrate surface is covered with an amorphous layer by ablating $\text{La}_2\text{Ti}_2\text{O}_7$ target, which is indicated by the vanishing RHEED pattern after this process step. Upon heating to 700°C the amorphous layer crystallizes and the streak pattern forms gradually. This solid state epitaxial step at 700°C is favored due to a small lattice mismatch between LaTiO_3 and KTaO_3 , which gives a clear diffraction pattern correspondence between the substrate and the crystallized layer. The crystallized layer enables successive homoepitaxial growth, which takes place at a lower temperature of 600°C. The heterostructures discussed in this work differ by the LaTiO_3 layer thickness deposited at 600°C. After the growth, the heterostructures are cooled to room temperature and are left to thermalize for about 12h. Subsequently, the structures are covered with a thin amorphous layer by ablating the $\text{La}_2\text{Ti}_2\text{O}_7$ target to prevent potential degradation of structures at ambient condition. We note that the growth conditions favor the stabilization of LaTiO_3 phase²⁵. To check the film crystal structure, we grow a thick LaTiO_3 layer with 735 pulses. Figure 1c depicts its x-ray diffraction pattern (green trace) featuring Laue fringes, which indicate a high crystalline film quality. Due to the similar lattice parameters of LaTiO_3 and KTaO_3 , the Bragg diffraction peak of LaTiO_3 is indiscernible due to the overlapped diffraction pattern of the substrate (blue trace). By fitting the position of the Laue fringes (red line) we determine the film thickness of 14 nm, which is used to estimate the thickness of thinner films from a given number of pulses as depicted in Fig. 1b for each process step. The stoichiometry of the structures checked with energy-dispersive X-ray spectroscopy was comparable with that of the target. We note

however that the exact stoichiometry of the structure can have an impact on the interface conductivity²⁶⁻²⁸.

B. Electrical Transport Characteristics

The transport characteristics of heterostructures are shown in Fig. 2. We employed a Physics Properties Measurement System (PPMS, Quantum Design) down to 2 K and adiabatic demagnetization refrigerator (ADR) stage, which is compatible with PPMS platform, to characterize the superconducting transition of heterostructures down to 150 mK. The samples are directly bonded with aluminum wires as depicted in Fig. 3a, so that they can be characterized along two orthogonal directions simultaneously. Figures 2a and 2b depict exemplary temperature dependence of R_{xx} for three crystal orientations. Consistent with previous reports, the (111)-oriented heterostructure has a higher superconducting transition temperature than the (110)-oriented heterostructures^{15-17,19}. More importantly, we observe that the onset temperature of superconducting phase T_c^{onset} strongly depends on the thickness of LaTiO_3 layer. Such an impact of top layer thickness on the superconducting state hasn't been reported yet. Figure 2c depicts that T_c^{onset} increases with decreasing thickness of the LaTiO_3 layer. Such behavior is observed for both (110) and (111) oriented heterostructures. Following this finding, we measured one of the (001)-oriented heterostructures with a 1.7 nm thick LaTiO_3 layer in a dilution refrigerator at temperature down to 40 mK, but did not observe superconducting transition. The absence of superconducting phase for (001) oriented heterostructures is consistent with previous report¹⁹. To check the conductance of LaTiO_3 layer, we grew a 2.6 nm thin LaTiO_3 layer on both GdScO_3 and NdScO_3 substrates according to the growth procedure of Fig. 1. The resistance of such structures at room temperature was on the order of 10^6 Ohm.

Figure 3b compares the resistance values of heterostructures above ($T = 2$ K, left panel) and below ($T = 150$ mK, right panel) the superconducting transition. It is noticeable

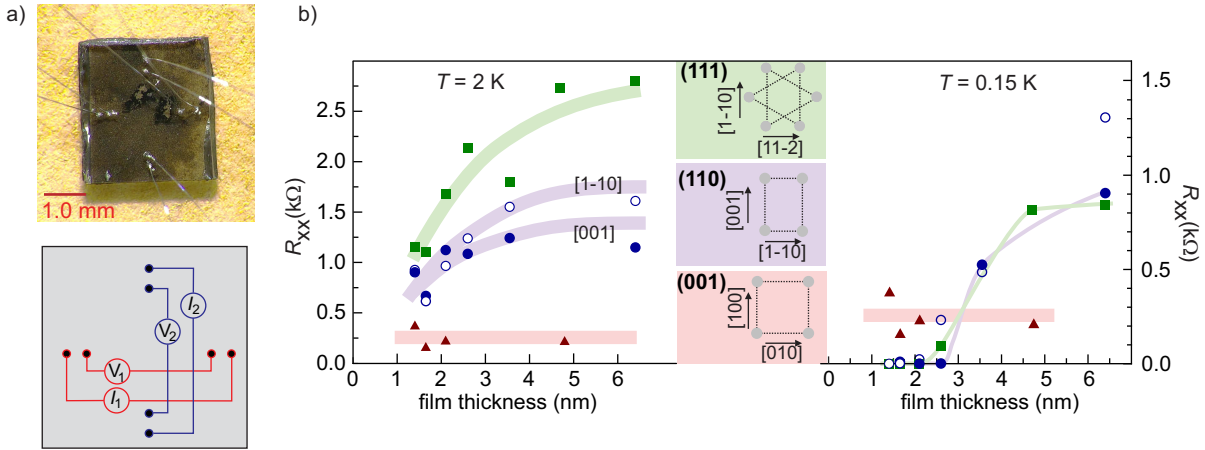


FIG. 3. a) Photograph of a sample with attached wires to measure temperature dependence of sample resistance. Shown also is the scheme of electrical circuit sample connection. Multi-channel source-measurement unit of PPMS is used to measure two orthogonal crystal directions simultaneously. b) Resistance at zero magnetic field at $T = 2\text{ K}$ (above superconducting transition, left panel) and at $T = 150\text{ mK}$ (below superconducting transition, right panel) as a function of LaTiO₃ thickness. The color encodes the crystal orientation of heterostructures. Thin heterostructures with (110) and (111) crystal orientations show $R_{xx} = 0\text{ }\Omega$ at $T = 150\text{ mK}$. As LaTiO₃ thickness increases, the residual R_{xx} increases. The thick lines are guides to the eye.

that R_{xx} at $T = 2\text{ K}$ increases with increasing LaTiO₃ thickness for both the (111) and (110) oriented structures, while it remains almost constant for the (001)-oriented heterostructures. Such behavior points to the interface conductance rather than to the conductance in LaTiO₃ layer solely, in which case the resistance would decrease with increasing LaTiO₃ thickness. To further elucidate the properties of the heterostructures, we present in Fig. 4 the dependence of both the electron mobility and the charge carrier density on LaTiO₃ thickness. Charge carrier density n is estimated from the Hall effect measurements, while mobility μ is estimated from the sample conductance in zero magnetic field. Among the three crystal orientations, the (001)-oriented heterointerface has the highest electron mobility on the order of $250\text{ cm}^2\text{V}^{-1}\text{s}^{-1}$, which does not depend on the LaTiO₃ thickness. Both the electron mobility and the charge carrier density values are consistent with those obtained for LaTiO₃/KTaO₃ (001)-oriented structures grown by molecular beam epitaxy²⁴. For both the (110) and (111) oriented heterostructures the electron mobility shows a distinct behavior; it is the largest for thin structures, i.e. around $100\text{ cm}^2\text{V}^{-1}\text{s}^{-1}$, and decreases with increasing LaTiO₃ thickness, reaching a saturation value of around $30\text{ cm}^2\text{V}^{-1}\text{s}^{-1}$ above a LaTiO₃ thickness of 2 nm . By contrast the charge carrier density shows a fast increase with LaTiO₃ thickness by about a factor 1.5 (lower panel in Fig. 4) and saturates above 2 nm . This seems to be a common tendency for all three crystal orientations. An increase of the sheet charge carrier density n (Fig. 4b) and, at the same time, a decrease of T_c^{onset} with LaTiO₃ thickness (Fig. 2c) establishes an opposite tendency to the previous observations in KTaO₃-based superconducting structures, for which superconducting transition temperature increases with increasing n ^{19,20}. The presented results indicate an impact of epitaxial LaTiO₃ layer on the electronic properties of the interface, which also affects the superconducting regime as we discuss now.

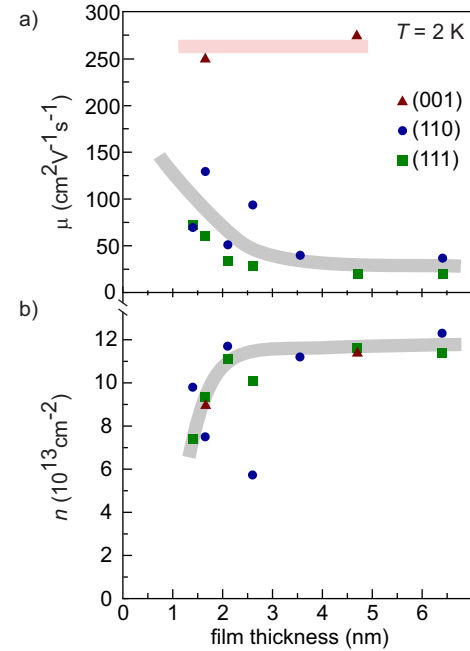


FIG. 4. Mobility (panel a)) and charge carrier density (panel b)) dependence on LaTiO₃ layer thickness at $T = 2\text{ K}$ for different heterostructure orientations. The charge carrier density is estimated from the transverse resistance R_{xy} (Hall effect), which changes linearly with the magnetic field B . Thick lines are guides to the eye.

Right panel in Fig. 3b depicts the dependence of R_{xx} at 150 mK (well below T_c^{onset}) on the LaTiO₃ thickness for all heterostructures. For the sake of comparison, it also contains data points for the high mobility (001) interface that does not become superconducting in our experiments. A well developed superconducting state characterized by $R_{xx} = 0\text{ }\Omega$ is

reached for both (110)- and (111)-oriented heterostructures but only with a thin LaTiO_3 layer. For thicker LaTiO_3 layers R_{xx} attains a non-zero value, which increases with increasing LaTiO_3 thickness. Furthermore, we detect an anisotropy for the (110)-oriented structures. Open symbols in the right panel depict R_{xx} values measured along the [1-10] direction at 150 mK. For 2.1 nm and 2.6 nm thick samples the superconductivity along [001] direction survives at 150 mK, while R_{xx} along [1-10] direction has a non-zero value. (In the Supplementary Information we show the temperature dependence of R_{xx} during superconducting transition for all samples.) By contrast to (110)-oriented structures, [1-10] and [11-2] crystal directions of (111)-oriented heterostructures appear to be equivalent. Since the heterostructures are grown in equivalent procedures, it allows us to conclude that a potential sample inhomogeneity cannot explain the anisotropy as observed in (110)-oriented structures. This surprising emergence of anisotropic behavior of R_{xx} below superconducting transition is perhaps related to the imminent electronic structure of the interface. Anisotropy for (110)-oriented heterostructures is reported for the normal conducting state of SrTiO_3 -based heterostructures and is related to a different arrangement of interface atoms along [001] and [1-10] directions^{29,30}. An indication of such an anisotropy in our (110)-oriented heterostructures might also appear in the normal conducting state. At $T = 2$ K, Figure 3b (left panel) depicts that R_{xx} along the [1-10] direction (open blue symbols) is larger than for the [001] direction (full blue symbols).

Beyond that, increasing the LaTiO_3 thickness affects the transport characteristics of both the (110)- and (111)-oriented heterostructures before superconducting transition. In fact, for structures with a thicker LaTiO_3 , one clearly observes some increase in $R_{xx} \propto \ln T$ indicating a contribution of the weak localization correction to the sample resistance (see Supplementary Information). This has also been observed in superconducting $\text{LaTiO}_3/\text{SrTiO}_3$ structures³¹. Conspicuously, when this localization behavior is strongly pronounced in our structures, $R_{xx} = 0 \Omega$ vanishes for (110) as well as for (111)-oriented structures, as seen in Supplementary Information. The (110) and (111) heterostructures feature a weak antilocalization behavior in magnetotransport, indicating a significance of spin-orbit coupling. Intriguingly, weak antilocalization is barely pronounced for non-superconducting (001)-oriented heterostructures (see Supplementary Information).

The observation of the superconducting transition being dependent on the KTaO_3 surface orientation is consistent with previous reports on superconductivity in KTaO_3 ¹⁵⁻¹⁹. This allows us to conclude that the superconducting phase in our structures involves the electronic states of KTaO_3 . At the same time the LaTiO_3 thickness dependence of the transport characteristics both in superconducting and normal state implies a non-trivial impact of the top layer on the electronic structure of the $\text{LaTiO}_3/\text{KTaO}_3$ heterointerface. In the vicinity of the junction, the Ta atoms are in a 5+ state, whereas Ti is in a 3+ state. This charge discontinuity can lead to charge redistribution between the LaTiO_3 and KTaO_3 layers adjacent to the interface, creating an interfacial conducting layer. One such mechanisms can be related to a so called polar catastro-

phe, which is based on compensation of the diverging electrostatic energy at the interface³². This mechanism has been considered for various SrTiO_3 and KTaO_3 based heterostructures and can be effective for (001) and (111) oriented structures, but is not obvious for (110) structures^{24,33-36}. Surface reconstruction and the modification of TiO_6 octahedra have also been considered for the emergence of conducting layers at the interface between band insulators and Mott insulators such as LaTiO_3 ³⁷⁻³⁹. Moreover, oxygen defects can contribute to the emergence of a conducting layer. It would require additional experimental and theoretical efforts to elucidate how each of those mechanisms is realized in our superconducting $\text{LaTiO}_3/\text{KTaO}_3$ structures. The interplay of those mechanisms will define the extension of the conducting layer, interaction between the LaTiO_3 and KTaO_3 layers, and consequently the total electronic structure.

CONCLUSION

In summary, we have grown epitaxial $\text{LaTiO}_3/\text{KTaO}_3$ heterostructures with (001), (110) and (111) crystal orientations and varying LaTiO_3 thickness. The (110)- and (111)-oriented heterostructures have a moderate electron mobility and a well developed superconducting state. The (001)-oriented heterostructures have the highest electron mobility with no indication of a superconducting transition. The LaTiO_3 layer has a non-trivial impact on the emergence of the superconducting phase. With increasing LaTiO_3 thickness the superconducting transition temperature decreases and a finite resistance remains below the transition. This behavior seems to correlate with the emergence of electron weak localization. Furthermore, for the (110)-oriented heterostructures we observe a regime when $R_{xx} = 0 \Omega$ along the [001] direction and non-zero for the [1-10] direction, thus establishing anisotropic superconductivity in $\text{LaTiO}_3/\text{KTaO}_3$ -heterostructures. Our result may pave the way to engineer superconducting interfaces and to integrate superconducting KTaO_3 interfaces with oxide materials.

SUPPLEMENTARY MATERIALS

See the supplementary material for additional details on superconducting transition, features of weak antilocalization behavior in the magnetic field and atomic force microscopy images.

ACKNOWLEDGMENTS

We would like to thank Dr. M. Kriener and Dr. M. Birch for fruitful discussion and careful reading of the manuscript. This work was supported by JSPS KAKENHI (22H04958). The work of E.S. is supported through Grants No. PGC2018-101355-B-I00 and No. PID2021-126273NB-I00 funded by MCIN/AEI/10.13039/501100011033 and by the ERDF “A way of making Europe”, and by the Basque Government

through Grant No. IT1470-22. The work of V.D. is supported by the National Science Center in Poland as a research project No. DEC-2017/27/B/ST3/02881.

- ¹A. Ohtomo and H. Y. Hwang, “A high-mobility electron gas at the LaAlO₃/SrTiO₃ heterointerface,” *Nature* **427**, 423–426 (2004).
- ²N. Reyren, S. Thiel, A. D. Caviglia, L. F. Kourkoutis, G. Hammerl, C. Richter, C. W. Schneider, T. Kopp, A.-S. Rüetschi, D. Jaccard, M. Gabay, D. A. Muller, J.-M. Triscone, and J. Mannhart, “Superconducting interfaces between insulating oxides,” *Science* **317**, 1196–1199 (2007).
- ³A. D. Caviglia, S. Gariglio, N. Reyren, D. Jaccard, T. Schneider, M. Gabay, S. Thiel, G. Hammerl, J. Mannhart, and J.-M. Triscone, “Electric field control of the LaAlO₃/SrTiO₃ interface ground state,” *Nature* **456**, 624–627 (2008).
- ⁴Y. A. Bychkov and E. I. Rashba, “Properties of a 2D electron gas with lifted spectral degeneracy,” *JETP Letters* **39**, 78–81 (1984).
- ⁵A. D. Caviglia, M. Gabay, S. Gariglio, N. Reyren, C. Cancellieri, and J.-M. Triscone, “Tunable Rashba spin-orbit interaction at oxide interfaces,” *Phys. Rev. Lett.* **104**, 126803 (2010).
- ⁶M. Ben Shalom, M. Sachs, D. Rakhmilevitch, A. Palevski, and Y. Dagan, “Tuning Spin-Orbit Coupling and Superconductivity at the SrTiO₃/LaAlO₃ Interface: A Magnetotransport Study,” *Phys. Rev. Lett.* **104**, 126802 (2010).
- ⁷G. Herranz, G. Singh, N. Bergeal, A. Jouan, J. Lesueur, J. Gázquez, M. Varela, M. Scigaj, N. Dix, F. Sánchez, and J. Fontcuberta, “Engineering two-dimensional superconductivity and Rashba spin-orbit coupling in LaAlO₃/SrTiO₃ quantum wells by selective orbital occupancy,” *Nature Communications* **6**, 6028 (2015).
- ⁸J. W. F. Venderbos, L. Savary, J. Ruhman, P. A. Lee, and L. Fu, “Pairing States of Spin- $\frac{3}{2}$ Fermions: Symmetry-Enforced Topological Gap Functions,” *Phys. Rev. X* **8**, 011029 (2018).
- ⁹L. P. Gor’kov and E. I. Rashba, “Superconducting 2D System with Lifted Spin Degeneracy: Mixed Singlet-Triplet State,” *Phys. Rev. Lett.* **87**, 037004 (2001).
- ¹⁰M. S. Scheurer and J. Schmalian, “Topological superconductivity and unconventional pairing in oxide interfaces,” *Nature Communications* **6**, 6005 (2014).
- ¹¹V. Kozii and L. Fu, “Odd-parity superconductivity in the vicinity of inversion symmetry breaking in spin-orbit-coupled systems,” *Phys. Rev. Lett.* **115**, 207002 (2015).
- ¹²S. Nakosai, Y. Tanaka, and N. Nagaosa, “Topological superconductivity in bilayer Rashba system,” *Phys. Rev. Lett.* **108**, 147003 (2012).
- ¹³S. H. Wemple, “Some Transport Properties of Oxygen-Deficient Single-Crystal Potassium Tantalate KTaO₃,” *Phys. Rev.* **137**, A1575–A1582 (1965).
- ¹⁴K. Ueno, S. Nakamura, H. Shimotani, H. T. Yuan, N. Kimura, T. Nojima, H. Aoki, Y. Iwasa, and M. Kawasaki, “Discovery of superconductivity in KTaO₃ by electrostatic carrier doping,” *Nature Nanotechnology* **6**, 408–412 (2011).
- ¹⁵Z. Chen, Z. Liu, Y. Sun, X. Chen, Y. Liu, H. Zhang, H. Li, M. Zhang, S. Hong, T. Ren, C. Zhang, H. Tian, Y. Zhou, J. Sun, and Y. Xie, “Two-Dimensional Superconductivity at the LaAlO₃/KTaO₃(110) Heterointerface,” *Phys. Rev. Lett.* **126**, 026802 (2021).
- ¹⁶C. Liu, X. Yan, D. Jin, Y. Ma, H.-W. Hsiao, Y. Lin, T. M. Bretz-Sullivan, X. Zhou, J. Pearson, B. Fisher, J. S. Jiang, W. Han, J.-M. Zuo, J. Wen, D. D. Fong, J. Sun, H. Zhou, and A. Bhattacharya, “Two-dimensional superconductivity and anisotropic transport at KTaO₃(111) interfaces,” *Science* **371**, 716–721 (2021).
- ¹⁷X. Hua, F. Meng, Z. Huang, Z. Li, S. Wang, B. Ge, Z. Xiang, and X. Chen, “Tunable two-dimensional superconductivity and spin-orbit coupling at the EuO/KTaO₃(110),” *npj Quantum Materials* **7**, 97 (2022).
- ¹⁸Z. Chen, Y. Liu, H. Zhang, Z. Liu, H. Tian, Y. Sun, M. Zhang, Y. Zhou, J. Sun, and Y. Xie, “Electric field control of superconductivity at the LaAlO₃/KTaO₃(111) interface,” *Science* **372**, 721–724 (2021).
- ¹⁹C. Liu, X. Zhou, D. Hong, B. Fisher, H. Zheng, J. Pearson, J. S. Jiang, D. Jin, M. R. Norman, and A. Bhattacharya, “Tunable superconductivity and its origin at KTaO₃ interfaces,” *Nature Communications* **14**, 951 (2023).
- ²⁰S. Mallik, G. C. Ménard, G. Saïz, H. Witt, J. Lesueur, A. Gloter, L. Benfatto, M. Bibes, and N. Bergeal, “Superfluid stiffness of a KTaO₃-based two-dimensional electron gas,” *Nature Communications* **13**, 4625 (2022).
- ²¹A. H. Al-Tawhid, J. Kanter, M. Hafeipour, D. P. Kumah, J. Shabani, and K. Ahadi, “Superconductivity and weak antilocalization at KTaO₃(111) interfaces,” *J. Electron. Mater.* **51**, 6305 (2022).
- ²²E. G. Arnault, A. H. Al-Tawhid, S. Salmani-Rezaie, D. A. Muller, D. P. Kumah, M. S. Bahramy, G. Finkelstein, and K. Ahadi, “Anisotropic superconductivity at KTaO₃(111) interfaces,” *Science Advances* **9**, eadf1414 (2023).
- ²³K. Momma and F. Izumi, “VESTA 3 for three-dimensional visualization of crystal, volumetric and morphology data,” *J. Appl. Crystallogr.* **44**, 1272–1276 (2011).
- ²⁴K. Zou, S. Ismail-Beigi, K. Kisslinger, X. Shen, D. Su, F. J. Walker, and C. H. Ahn, “LaTiO₃/KTaO₃ interfaces: A new two-dimensional electron gas system,” *APL Materials* **3**, 036104 (2015).
- ²⁵A. Ohtomo, D. A. Muller, J. L. Grazul, and H. Y. Hwang, “Epitaxial growth and electronic structure of LaTiO_x films,” *Applied Physics Letters* **80**, 3922–3924 (2002).
- ²⁶E. Breckenfeld, N. Bronn, J. Karthik, A. R. Damodaran, S. Lee, N. Mason, and L. W. Martin, “Effect of growth induced (non)stoichiometry on interfacial conductance in LaAlO₃/SrTiO₃,” *Phys. Rev. Lett.* **110**, 196804 (2013).
- ²⁷H. K. Sato, C. Bell, Y. Hikita, and H. Y. Hwang, “Stoichiometry control of the electronic properties of the LaAlO₃/SrTiO₃ heterointerface,” *Applied Physics Letters* **102**, 251602 (2013).
- ²⁸M. P. Warusawithana, C. Richter, J. A. Mundy, P. Roy, J. Ludwig, S. Paetel, T. Heeg, A. A. Pawlicki, L. F. Kourkoutis, M. Zheng, M. Lee, B. Mulcahy, W. Zander, Y. Zhu, J. Schubert, J. N. Eckstein, D. A. Muller, C. S. Hellberg, J. Mannhart, and D. G. Schlom, “LaAlO₃ stoichiometry is key to electron liquid formation at LaAlO₃/SrTiO₃ interfaces,” *Nature Communications* **4**, 2351 (2013).
- ²⁹A. Annadi, Q. Zhang, X. Renshaw Wang, N. Tuzla, K. Gopinadhan, W. M. Lü, A. Roy Barman, Z. Q. Liu, A. Srivastava, S. Saha, Y. L. Zhao, S. W. Zeng, S. Dhar, E. Olsson, B. Gu, S. Yunoki, S. Maekawa, H. Hilgenkamp, T. Venkatesan, and Ariando, “Anisotropic two-dimensional electron gas at the LaAlO₃/SrTiO₃ (110) interface,” *Nature Communications* **4**, 1838 (2013).
- ³⁰Z. Wang, Z. Zhong, X. Hao, S. Gerhold, B. Stöger, M. Schmid, J. Sánchez-Barriga, A. Varykhalov, C. Franchini, K. Held, and U. Diebold, “Anisotropic two-dimensional electron gas at SrTiO₃ (110),” *Proceedings of the National Academy of Sciences* **111**, 3933–3937 (2014).
- ³¹J. Biscaras, N. Bergeal, A. Kushwaha, T. Wolf, A. Rastogi, R. Budhani, and J. Lesueur, “Two-dimensional superconductivity at a Mott insulator/band insulator interface LaTiO₃/SrTiO₃,” *Nature Communications* **1**, 89 (2010).
- ³²N. Nakagawa, H. Y. Hwang, and D. A. Muller, “Why some interfaces cannot be sharp,” *Nature Materials* **5**, 204–209 (2006).
- ³³A. Ohtomo, D. A. Muller, J. L. Grazul, and H. Y. Hwang, “Artificial charge-modulation in atomic-scale perovskite titanate superlattices,” *Nature* **419**, 378–380 (2002).
- ³⁴Y. Hotta, T. Susaki, and H. Y. Hwang, “Polar Discontinuity Doping of the LaVO₃/SrTiO₃ Interface,” *Phys. Rev. Lett.* **99**, 236805 (2007).
- ³⁵P. Moetakef, T. A. Cain, D. G. Ouellette, J. Y. Zhang, D. O. Klenov, A. Jantotti, C. G. Van de Walle, S. Rajan, S. J. Allen, and S. Stemmer, “Electrostatic carrier doping of GdTiO₃/SrTiO₃ interfaces,” *Applied Physics Letters* **99**, 232116 (2011).
- ³⁶A. H. Al-Tawhid, D. P. Kumah, and K. Ahadi, “Two-dimensional electron systems and interfacial coupling in LaCrO₃/KTaO₃ heterostructures,” *Applied Physics Letters* **118**, 192905 (2021).
- ³⁷S. Okamoto and A. J. Millis, “Electronic reconstruction at an interface between a Mott insulator and a band insulator,” *Nature* **428**, 630 (2004).
- ³⁸S. Okamoto, A. J. Millis, and N. A. Spaldin, “Lattice Relaxation in Oxide Heterostructures: LaTiO₃/SrTiO₃ Superlattices,” *Phys. Rev. Lett.* **97**, 056802 (2006).
- ³⁹H. Ishida and A. Liebsch, “Origin of metallicity of LaTiO₃/SrTiO₃ heterostructures,” *Phys. Rev. B* **77**, 115350 (2008).